NUMERICAL STUDIES OF FEED CYCLING IN A CSTR

Karel KLUSÁČEK*, Peter Lewis SILVESTON and Robert Ross HUDGINS

Department of Chemical Engineering,
University of Waterloo, Waterloo, Ontario, Canada N2L 3G1

Received September 11, 1989
Accepted February 3, 1990

A numerical study of feed composition cycling (periodic operation) of stoichiometrically simple reactions described by Langmuir–Hinshelwood or Eley–Rideal kinetics reveal that although time-average production rates may be higher than the corresponding steady-state ones at the same time-average feed composition, they do not exceed the maximum steady-state rates at a given space velocity. This behaviour is explained by the dynamics of surface concentrations of adsorbed species during a cycle. Although these findings support other numerical studies, they are at variance with experimental observations. Thus, there is a need to develop more sophisticated kinetic models for the prediction of dynamic behaviour of heterogeneous catalytic systems.

Forced periodic operation of catalytic reactors has attracted increasing attention in recent years. It has been shown both theoretically and experimentally (see for example the reviews by Bailey[1], and Silveston and Hudgins[2]) that reaction rate and/or selectivity may be significantly increased by means of periodic cycling of system variables, usually feed composition.

For simple reactions, an increase in the conversion (or global reaction rate) may be accomplished easily by increasing the catalyst loading in a reactor but this is sometimes undesirable for complex reactions because of unfavourable selectivity. An alternative technique is to use a catalyst with greater selectivity or to choose another kind of reactor or another type of reactor operation, such as periodic. Simple reactions are nevertheless useful for a general theoretical analysis of transient reactor behaviour; the conclusions obtained may be extended to complex reactions systems.

For possible exploitation of forced feed cycling operation in practice it is necessary to known whether the results obtained are superior to those obtained under (optimum) steady-state operation. The question of improvement of CSTR performance by the dynamic control of reactor feed has been addressed by Schädlich et al.[3]. They attempted to predict whether it is possible to improve conversion or selectivity by periodic feed cycling; however, no comparison was made with optimum steady-state reactor operation. Nowobilski et al.[4] recently observed that in a few particular

* On leave from the Institute of Chemical Process Fundamentals, Czechoslovak Academy of Sciences, 165 02 Prague 6, Czechoslovakia.

catalytic reactions, periodic operation does not cause the selectivity or the mean reaction rate to exceed their respective optimum steady-state values.

The purpose of this paper is to examine the question of improvement using modeling of a periodically operated CSTR for some simple heterogeneous catalytic reactions assuming classical Langmuir–Hinshelwood and Eley–Rideal mechanisms. We restrict our consideration to feed composition as the forcing variable. Special attention is paid to the behaviour of the model under time-average feed composition corresponding to the optimum steady state.

THEORETICAL

In this work, the reaction,

$$A + 2B \rightarrow C$$

is considered where A, B are gaseous reactants and C is gaseous product. It is assumed that the reaction can proceed via Langmuir–Hinshelwood or Eley-Rideal mechanisms.

Langmuir–Hinshelwood Mechanism

$$A + S \underset{k_1'}{\overset{k_1}{\rightleftharpoons}} A \,.\, S \qquad (1a)$$

$$2B + S \underset{k_2'}{\overset{k_2}{\rightleftharpoons}} B_2 \,.\, S \qquad (1b)$$

$$A \,.\, S + B_2 \,.\, S \xrightarrow{k_3} C + 2S \qquad (1c)$$

Reactants A and B are reversibly adsorbed on active centres S (steps *1a*, *1b*) and both adsorbed components A . S and B_2 . S react in the irreversible step (*1c*) producing the gaseous product C.

Eley–Ridel Mechanism

$$A + S \underset{k_1'}{\overset{k_1}{\rightleftharpoons}} A \,.\, S \qquad (2a)$$

$$A \,.\, S + 2B \xrightarrow{k_3} C + S \qquad (2b)$$

In this mechanism the adsorption of A (step *2a*) is followed by the surface reaction between adsorbed A . S and two molecules of B directly from the gas phase. For simplicity the above steps are assumed to be elementary in both mechanisms. Several other stoichiometries were also studied in this work and those are mentioned in conclusion.

Mass Balance Equations

By denoting the gaseous components as

$$A = A_1 , \quad B = A_2 , \quad C = A_3$$

and the surface somponents as

$$S = A_4 , \quad A . S = A_5 , \quad B_2 . S = A_6$$

the dimensionless mass balances of CSTR (assuming negligible transport effects) take the following form[5] for the reactor bulk

$$(da_i/d\tau) = a_i^0 - (\sigma/\sigma^0)\, a_i + \phi\varrho_i , \quad i = 1, 2, 3 \tag{3}$$

and for the catalyst surface

$$(da_j/d\tau) = \varrho_j , \quad j = 4, 5, 6 \text{ (for the L–H mechanism)}$$
$$j = 4, 5 \quad \text{(for the E–R mechanism)} . \tag{4}$$

Definition of the variables used in Eqs (*3*) and (*4*) are summarized in Table I. The space velocity at the reactor outlet, σ, may be expressed as a function of the inlet space velocity, σ^0, by the relation

$$\sigma = \sigma^0(1 + \phi \sum_{i=1}^{3} \varrho_i) . \tag{5}$$

Mass balance Eqs (*3*) and (*4*) are complemented by the initial conditions for

$$\tau = 0 , \quad a_i(\tau) = a_i(0) , \quad i = 1, 2, 3$$
$$a_j(\tau) = a_j(0) , \quad j = 4, 5, 6 \text{ (for the L–H mechanism)}$$
$$j = 4, 5 \quad \text{(for the E–R mechanism)} . \tag{6}$$

The form of the dimensionless rates ϱ_i, ϱ_j is given in Table II and the expressions for dimensionless rate constants are summarized in Table III. As is apparent from the table, the dimensionless rate constants depend on the inlet space velocity σ^0. The numerical values of constants given in Table III correspond to $\sigma^0 = 1\ s^{-1}$.

For the presentation of results, it is useful to define the normalized rate of product formation, ϱ, as the ratio of the actual and maximum possible rates ϱ_3. As is evident from Table II, the maximum possible rate of product formation for the L–H mechanism is reached at $a_5 = a_6 = 0{\cdot}5$ and for the E–R mechanism at $a_2 = a_5 = 1$. Normalized

TABLE I
Dimensionless variables

Variable	Definition
concentration of gaseous A_i (mole fraction)	$a_i = c_i/c_T$
concentration of surface A_j	$a_j = c_j/_{jL}$
capacity factor	$\phi = Wc_L/(Vc_T)$
time	$\tau = t\sigma^0$

TABLE II
Dimensionless rates of formation

Rate	L–H model	E–R model
ϱ_1	$-\varkappa_1 a_1 a_4 + \varkappa'_1 a_5$	$-\varkappa_1 a_1 a_4 + \varkappa'_1 a_5$
ϱ_2	$-2\varkappa_2 a_2^2 a_4 + 2\varkappa'_2 a_6$	$-2\varkappa_3 a_5 a_2^2$
ϱ_3	$\varkappa_3 a_5 a_6$	$\varkappa_3 a_5 a_2^2$
ϱ_4	$\varrho_1 + 1/2\varrho_2 + 2\varrho_3$	$\varrho_1 + \varrho_3$
ϱ_5	$-(\varrho_1 + \varrho_3)$	$-(\varrho_1 + \varrho_3)$
ϱ_6	$-(1/2\varrho_2 + \varrho_3)$	not used

TABLE III

Constant	L–H model, (value)	E–R model, (value)
$\varkappa_1$	$(c_T/\sigma^0)\, k_1$, (1·0)	$(c_T/\sigma^0)\, k_1$, (1·0)
$\varkappa_2$	$(c_T^2/\sigma^0)\, k_2$, (0·3)	not used
$\varkappa_3$	$(c_L/\sigma^0)\, k_3$, (0·1)	$(c_T^2/\sigma^0)\, k_3$, (0·1)
$\varkappa'_1$	$(1/\sigma^0)\, k'_1$, (0·05)	$(1/\sigma^0)\, k'_1$, (0·05)
$\varkappa'_2$	$(1/\sigma^0)\, k'_2$, (0·1)	not used

steady-state rates are expressed as follows:

$$\varrho = 4a_5a_6 \tag{7}$$

for the L–H mechanism, and

$$\varrho = a_2^2a_5 \tag{8}$$

for the E–R mechanism.

Concentration Cycling

Variables introduced by concentration cycling are illustrated in Fig. 1. In this study, only simple cycling of two reactants (A_1 and A_2) in the feed has been considered. The rectangular concentration change of both reactants occurs simulaneously but in opposite directions. The period length is τ_p; the symmetry of the period is given by split γ and the difference between higher and lower concentrations is the amplitude, α. The time-average feed concentrations are given by the relation

$$a^0_{i,M} = \gamma a^0_{i,I} + (1 - \gamma)\, a^0_{i,II}\,, \quad i = 1, 2\,, \tag{9}$$

where $a^0_{i,I}$ and $a^0_{i,II}$ are the inlet concentrations of components A_1 and A_2 in the first and second parts of the period respectively (see Fig. 1).

The periodic performance of a CSTR can be evaluated by means of the time-average normalized rate, ϱ_M, given as follows

$$\varrho_M = (1/\tau_p) \int_{n\tau_p}^{(n+1)\tau_p} \varrho \, d\tau\,, \tag{10}$$

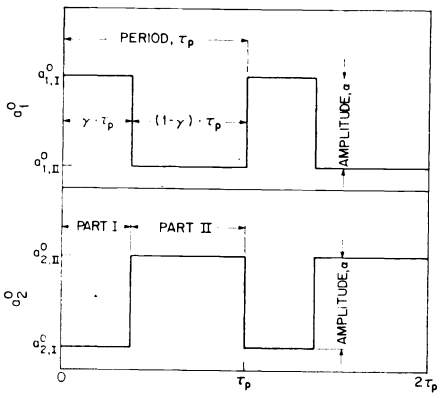

FIG. 1

Schematic of periodic operation defining variables: α, γ and τ_p

where n is any number greater than the minimum number of cycles necessary to establish cycle-invariant behaviour of a CSTR (i.e. consecutive outlet cycles are identical). Similarly, the time-average outlet concentrations of individual components are defined as

$$a_{i,M} = (1/\tau_p) \int_{n\tau_p}^{(n+1)\tau_p} a_i \, d\tau \,, \quad (i = 1, \ldots, 6 \text{ for the L–H mechanism}) \quad (i = 1, \ldots, 5 \text{ for the E–R mechanism}) \,. \qquad (11)$$

RESULTS AND DISCUSSION

Steady State

In the steady state, the derivatives (accumulation terms) on the left-hand side of Eqs (*3*) and (*4*) are equal to zero and the set of coupled differential equations thus becomes a set of nonlinear algebraic equations. This set has been solved numerically by the use of modification of Powell's hybrid algorithm[6] for a series of ratios of a_1^0/a_2^0 in the feed and for different values of the inlet splace velocity, σ^0. Fig. 2 presents results for the Langmuir-Hinshelwood mechanism and Fig. 3 for the Eley–Rideal mechanism. In both figures, the dimensionless steady-state rates ϱ_{ss}, given also by

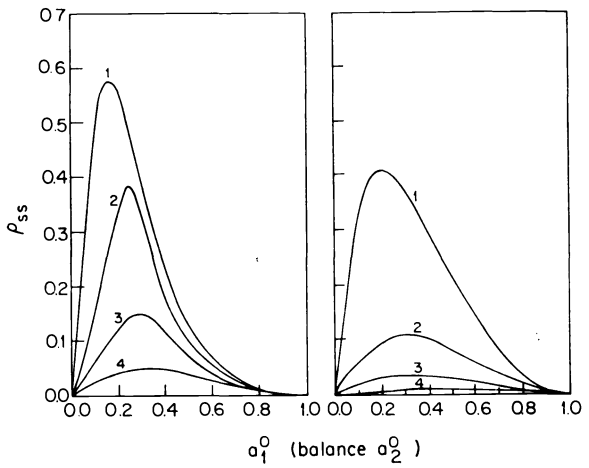

FIG. 2

Dimensionless steady-state rates, ϱ_{SS}, for Langmuir–Hinshelwood kinetics at different space velocities, σ^0 (in s^{-1}) 1 1 . 10^6, 2 0·1, 3 0·03, 4 0·01

FIG. 3

Dimensionless steady-state rates, ϱ_{SS}, for Eley–Rideal kinetics at different space velocities, σ° (in s^{-1}): 1 1 . 10^6, 2 0·1, 3 0·03, 4 0·01

Eqs (7) and (8), attain maxima at intermediate values of the reactant ratios a_1^0/a_2^0. The ratios at the maxima correspond to the optimum reactor feed composition. These shift with decreasing space velocity to $a_1^0/a_2^0 = 0{\cdot}5$, the stoichiometric feed ratio. This is the limit being approached roughly by the curves labelled 4 in Figs 2 and 3.

Optimum steady-state (OSS) feed compositions $(a_1^0/a_2^0)_{oss}$ and their corresponding rates ϱ_{oss} are summarized in Table IV. The values of ϱ_{oss} provide benchmarks for measuring the superiority of periodic operation over steady state at any space velocity, σ^0.

Periodic Feed Cycling

To obtain the transient CSTR behaviour, the system of dynamic mass balances (Eqs (3) and (4)) has been solved numerically for the initial conditions (Eq. (6)) using Gear's algorithm[7]. Variables considered were period (τ_p), split (γ) and amplitude (α) of the feed composition waves.

Steady-state and periodic performances of a CSTR are compared in Fig. 4 (for the L–H mechanism) and Fig. 5 (for the E–R mechanism). Figs 4a and 5a show the results of composition cycling as the ratio of the time-average rate ϱ_M to the steady-state rate ϱ_{ss} at the same time-average feed composition used in cycling ($a_{1,M}^0/a_{2,M}^0 = 0{\cdot}5$). Figs 4b and 5b show additional results in the cycling mode for a time-average feed composition equal to optimum steady state ($a_{1,M}^0/a_{2,M}^0 = 0{\cdot}3/0{\cdot}7$ in Fig. 4b and $a_{1,M}^0/a_{2,M}^0 = 0{\cdot}32/0{\cdot}68$ in Fig. 5b).

For the Langmuir–Hinshelwood mechanism, periodic operation can significantly increase the reaction rate relative to the corresponding steady state (Fig. 4a). Depending on the amplitude and the period used, the time-average rate ϱ_M may exceed the corresponding steady-state rate by more than 60%. However, this enhanced rate never exceeds the optimum steady-state rate at a constant space velocity as ma ybe seen by comparing the maximum ϱ_M following from Fig. 4a. In this figure, $\varrho_M/\varrho_{SS} = 1{\cdot}62$ for $\alpha = 1{\cdot}0$, $\tau_p = 10$ and $\sigma^0 = 0{\cdot}03\ s^{-1}$. The steady-state rate, ϱ_{SS}, at this space

TABLE IV
Optimum steady states

σ^0, s^{-1}	L–H model		E–R model	
	$(a_1^0/a_2^0)_{oss}$	ϱ_{oss}	$(a_1^0/a_2^0)_{oss}$	ϱ_{oss}
$1 . 10^6$	0·16/0·84	0·586	0·18/0·82	0·407
$1 . 10^{-1}$	0·26/0·74	0·397	0·30/0·70	0·118
$3 . 10^{-2}$	0·30/0·70	0·168	0·32/0·68	0·042
$1 . 10^{-2}$	0·32/0·68	0·061	0·33/0·67	0·015

velocity and feed composition ($a_1^0/a_2^0 = 0{\cdot}5/0{\cdot}5$) is $\varrho_{SS} = 0{\cdot}067$, (curve 3 in Fig. 2) and $\varrho_M = 0{\cdot}067 \,.\, 1{\cdot}62 = 0{\cdot}109$ which is considerably lower than ϱ_{OSS} in Table IV for this space velocity ($\varrho_{OSS} = 0{\cdot}168$ for $\sigma^0 = 0{\cdot}03\ s^{-1}$). A more detailed comparison of periodic operation with optimum steady state is given in Fig. 13.

Fig. 4a shows that maximum enhancement is reached using the maximum amplitude $\alpha = 1{\cdot}0$ (i.e. bang-bang operation, that is using pure reactants A_1 and A_2) and at period $\tau_p \approx 10$. As τ_p approaches zero, mixing in a CSTR smooths the feed disturbances and reactor approaches steady state. This behaviour differs from that of a plug flow reactor, in which relaxed steady states with high average rates ϱ_M are predicted[8-10]. With the increasing period, the rate approaches the limit referred to by Horn and Bailey[8] as quasi steady state. At high amplitudes ($\alpha = 0{\cdot}6$, $0{\cdot}8$, and $1{\cdot}0$) and short periods, the reactor performance significantly exceeds the corresponding quasi steady state while at low amplitudes, the rate monotonically moves to the

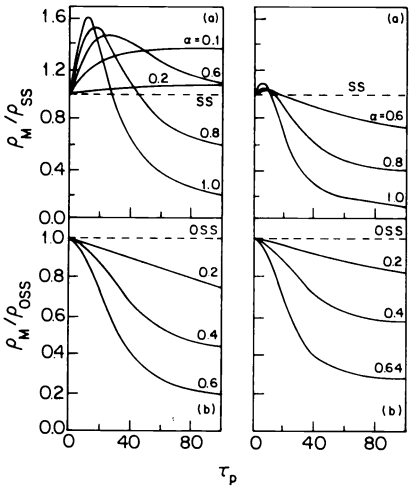

FIG. 4

Time-average rates of product formation for feed composition cycling as a function of period, τ_p, and amplitude, α, at split $\gamma = 0{\cdot}5$; a around a reactant ratio $a^0_{1,M}/a^0_{2,M} = 0{\cdot}5/0{\cdot}5$; b around a reactant ratio $a^0_{1,M}/a^0_{2,M} = 0{\cdot}3/0{\cdot}7$, corresponding to the optimum steady state. Langmuir–Hinshelwwod kinetics assumed

FIG. 5

Time-average rates of product formation for feed composition cycling as a function of period, τ_p, and amplitude, α, at split $\gamma = 0{\cdot}5$; a around a reactant ratio $a^0_{1,M}/a^0_{2,M} = 0{\cdot}5/0{\cdot}5$; b around a reactant ratio $a^0_{1,M}/a^0_{2,M} = 0{\cdot}32/0{\cdot}68$, corresponding to the optimum steady state. Eley–Rideal kinetics assumed

quasi steady state (not shown) as the period increases. Quasi steady states depend on amplitude, and this explains the different asymptotes in Figs 4 and 5.

Fig 4b shows the calculations for the L–H model for cycling around a time-average composition equal to the feed composition giving the maximum (optimum) rate ($a_1^0/a_2^0 = 0{\cdot}3/0{\cdot}7$, $\sigma^0 = 0{\cdot}03\ s^{-1}$). In contrast to cycling far from this optimum feed composition, cycling at the optimum-steady-state composition leads to a loss of reactor performance. The time-average rate ϱ_M never exceeds the optimum-steady--state rate, ϱ_{OSS}. However, as the figure shows, the ϱ_{OSS} is approached as τ_p approaches zero because at $\tau_p = 0$, the system is at steady state. The time-average dimensionless rate falls off with increasing period, regardless of amplitude.

Similar results are observed for the Eley–Rideal mechanism as is apparent from Fig. 5a. The main difference between mechanisms is that the E–R mechanism shows very little rate improvement as a result of cycling away from the optimum steady state (Fig. 5a). Behaviour of the system under cycling at the optimum steady-state composition is rather similar for both L–H and E–R mechanisms (cf. Figs 4b and 5b).

Thus, a comparison of forced periodic feed cycling with optimum steady-state operation shows lower reaction rates at all feed compositions for both considered mechanisms. Improved reactor performance illustrated in Figs 4a and 5a occurs only relative to suboptimum steady-state rates at a given space velocity.

An explanation of the above observations lies in the dynamics of processes on the catalyst surface and in the CSRT gas phase under forced feed cycling. Various gas-phase and surface transitens are shown in Figs 6 to 9 during cycling at the cycle--invariant state for the L–H mechanism. Figs 6 and 7 illustrate the system behaviour in one cycle for feed cycling aroung a reactant ratio $a_1^0/a_2^0 = 0{\cdot}5/0{\cdot}5$. Transients plotted in Figs 6 and 7 correspond to the maximum in the curve for $\alpha = 1{\cdot}0$ of Fig. 4a at $\tau_p = 10$, $\gamma = 0{\cdot}5$. The switching of the inlet stream composition is evident from Fig. 6a, b. Proportionality of the dimensionless rate to the product of the surface concentrations a_5 and a_6 explains the wide swings in this rate during a cycle. At the beginning of the cycle, after the switch from pure A_2 to pure A_1, both surface components A_5 and A_6 are present in relatively high concentration (Fig. 6c) and the value of ϱ is high (Fig. 6a). With increasing time, the surface concentration a_6 rapidly decreases because the feed does not contain A_2 and component A_6 is consumed in the reaction. On the other hand, the concentration a_5 of strongly adsorbed component A_1 (see values of constants in Table III) increases sharply. This change in surface concentrations leads to a decrease of the rate ϱ which falls to zero for $\tau \sim 3$ when A_6 becomes exhausted. At $\tau = 5$, the feed composition changes from pure A_1 to pure A_2. The surface storage of component A_5 is very high becuase of the strong adsorption of A_1 and both surface concentrations remain relatively high in the second part of the cycle (Fig. 6d) even in the absence of A_1 in the feed. The presence of both surface components leads to the high value of the normalized rate ϱ (Fig. 6b).

The trajectory of the surface concentrations corresponding to the cycle in Fig. 6 is shown in Fig. 7. The cycle begins at point P_1 and its progress with respect to surface concentration is charted by arrows to point P_2, which correspons to the mid-point of the cycle ($\tau = 5$). The return half-cycle is illustrated in the trajectory between the points P_2 and P_1. The dimensionless rate ϱ is highest for the surface composition given by point P_3 (where $a_5 = a_6 = 0{\cdot}5$) and decreases with increasing distance from this point. The dashed curves in Fig. 7 correspond to the constant value of the product $(4a_5a_6)$ which is the normalized rate according to Eq. (*7*). Curve 1 corresponds to $\varrho_{SS} = 0{\cdot}067$ which is the steady-state for the time-average feed composition. Curve 2 corresponds to time-average rate $\varrho_M = 0{\cdot}109$ in the cycle. It is significantly higher than the corresponding steady-state rate (curve 1). Points S shows the steady-state surface concentrations and point M corresponds to the time-average concentrations $a_{5,M}$ and $a_{6,M}$ in the cycle (Eq. (*11*)). This point is not on curve 2 because the time-average rate ϱ_M (Eq. (*10*)) is given by the mean value of the product of the surface concentrations $(4a_5a_6)$ and not by the value of the product of the mean surface concentrations.

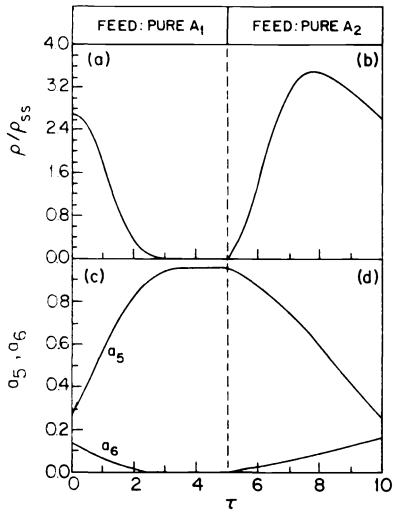

FIG. 6

Feed composition cycling at a reactant ratio different from that for the optimum steady state; a, b ratio of normalized rates ϱ/ϱ_{SS} and c, d surface concentrations a_5, a_6 in the cycle. Langmuir–Hinshelwood kinetics assumed; conditions: $\alpha = 1{\cdot}0$, $\tau_p = 10$, $\gamma = 0{\cdot}5$, $\sigma^0 = 0{\cdot}03\ s^{-1}$, $a^0_{1,M}/a^0_{2,M} = 0{\cdot}5/0{\cdot}5$

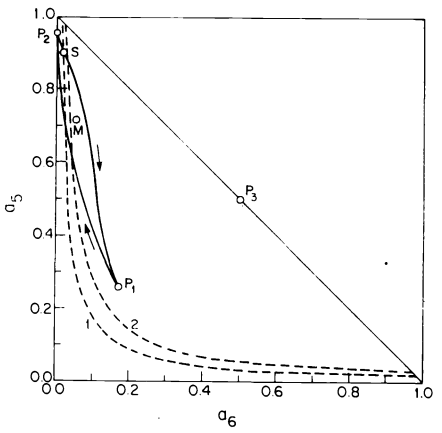

FIG. 7

Forced feed compoision cycling out of the optimum steady state; phase-plane trajectory of surface concentrations a_5 and a_6 during feed composition cycling as in Fig. 6 (Langmuir–Hinshelwood mechanism)

Figs 8 and 9 show the reaction behaviour under cycling for a time-average feed composition equal to the optimum steady-state composition ($a_1^0/a_2^0 = 0{\cdot}3/0{\cdot}7$). The points and curves in Fig. 9 are analogous to those in Fig. 7. As is apparent from Fig. 9, the mean surface concentration in the cycle (represented by the point M) is considerably closer to the point P_3 than the optimum steady-state concentrations (point S). However, the time-average rate $\varrho_M = 0{\cdot}091$ (curve 2) is significantly lower than the optimum steady-state rate $\varrho_{OSS} = 0{\cdot}168$ (curve 1). The explanation can be seen in Figs 8c, d. Surface concentrations a_5 and a_6 are sometimes very high during the cycle but never simultaneously – the necessary condition for a high rate ϱ.

Calculations of the Eley–Rideal mechanism of the reaction are shown in Figs 10 and 11 for cycling with the mean time-average feed composition equal to the optimum steady state ($a_1^0/a_2^0 = 0{\cdot}32/0{\cdot}68$). Since A_2 is not adsorbed in the E–R mechanism, a plot of surface concentrations a_5 vs a_6 would compress all the cycling trajectories onto the a_5 axis. Therefore, an a_2–a_5 plot is used, showing the surface concentration of adsorbed A_1 (a_5) vs the gas-phase concentration of A_2 (a_2).

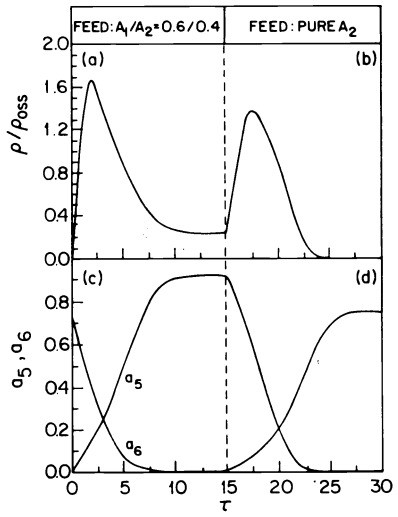

FIG. 8

Feed composition cycling at the optimum steady-state feed composition; a, b ratio of normalized rates ϱ/ϱ_{OSS} and c, d surface concentrations a_5, a_6 in the cycle. Langmuir–Hinshelwood mechanism assumed; conditions: $\alpha = 0{\cdot}6$, $\tau_p = 30$, $\gamma = 0{\cdot}5$, $\sigma^0 = 0{\cdot}03\ s^{-1}$, $a^0_{1,M}/a^0_{2,M} = 0{\cdot}3/0{\cdot}7$

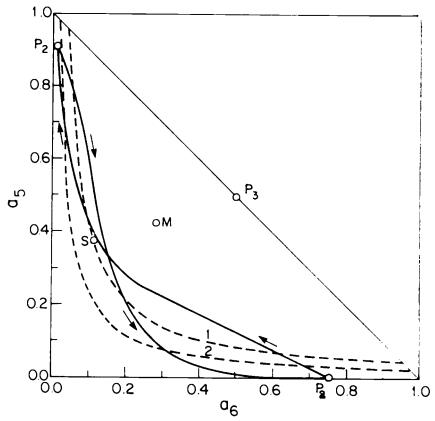

FIG. 9

Forced feed composition cycling in the optimum steady state; phase-plane trajectory of surface concentrations a_5 and a_6 during feed composition cycling as in Fig. 8 (Langmuir–Hinshelwood mechanism)

The switching of inlet stream composition is obvious from Figs 10a, b. The dimensionless rate ϱ is for E–R mechanism given by the product $a_2^2 a_5$ (Eq. (8)), and its change is shown in Figs 10a, b, while the changes of concentrations a_2 and a_5 are given in Figs 10c, d. Their trajectory in the cycle is shown by the arrows in Fig. 1; P_1 denotes the beginning and end and P_2 the mid-point of the cycle ($\tau = 15$). The dashed curves in Fig. 11 show the dimensionless rate ϱ (curve 1) for the optimum feed composition ($\varrho_{OSS} = 0{\cdot}042$), and the time-averaged rate ϱ_M for cycling around this feed composition (curve 2) $\varrho_M = 0{\cdot}021$. Point S corresponds to concentrations a_2 and a_5 at the optimum steady-state feed composition, while point M is given by the time-average concentrations $a_{2,M}$ and $a_{5,M}$ in the cycle. The closer a point is to the point with coordinates $a_2 = a_5 = 1$ (i.e. upper right corner), the higher is the corresponding rate ϱ. Nevertheless, as with the L–H mechanism (Fig. 9), the highest concentrations of the reactants a_2 and a_5 during the cycle are out of phase (see Figs 10c, d) and the net result is that ϱ_M is lower than ϱ_{OSS}.

Observations similar to those shown in Figs 6 to 11 have also been obtained for

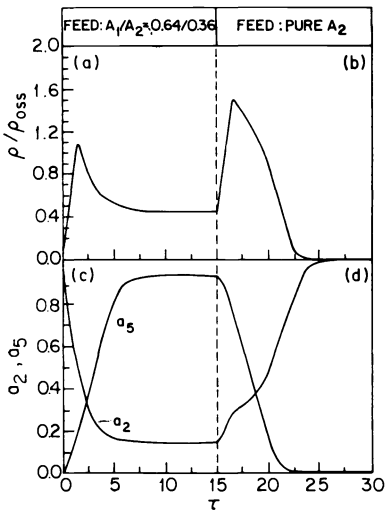

FIG. 10

Feed composition cycling at the optimum steady-state feed composition; a, b ratio of normalized rates ϱ/ϱ_{OSS} and c, d concentrations a_2, a_5 in the cycle. Eley–Rideal mechanism assumed; conditions: $\alpha = 0{\cdot}64, \tau_p = 30$, $\gamma = 0{\cdot}5$, $\sigma^0 = 0{\cdot}03\ s^{-1}$, $a_{1,M}/a^0_{2,M} = 0{\cdot}32/0{\cdot}68$

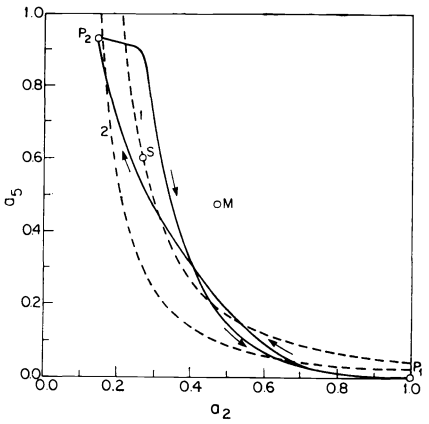

FIG. 11

Forced feed composition cycling in the optimum steady state; phase-plane trajectory of concentrations a_2 and a_5 during feed composition cycling as in Fig. 10 (Eley–Rideal mechanism)

other space velocities, different values of the cycle split γ (i.e. for asymmetric cycles) and various feed compositions (see Table IV). The enhancement of the reaction rate by the periodic operation may be considerable if the time-average feed composition is different from the optimum steady-state feed composition. However, compared with optimum steady-state operation, the rate enhancement under periodic operation appears never to exceed the maximum optimum steady-state rate for the above models. By this standard, the worst results under periodic operation are obtained at the time-average feed composition equal to the optimum steady state as is illustrated in Fig. 12 (see minima of the curves). This figure summarizes calculations for L–H (Fig. 12a) and E–R (Fig. 12b) mechanisms for different feed compositions. A comparison between time-average and steady-state rates was shown in Figs 4 and 5 for a single feed composition but as a function of period.

When compared with the optimum steady-state rates $\varrho_{OSS} = 0{\cdot}168$ (L–H model) and $\varrho_{OSS} = 0{\cdot}042$ (E–R model), (for $\sigma^\circ = 0{\cdot}03\ s^{-1}$, see Table IV), the time-average dimensionless rates for periodic operation are always lower, as may be seen in Fig. 13.

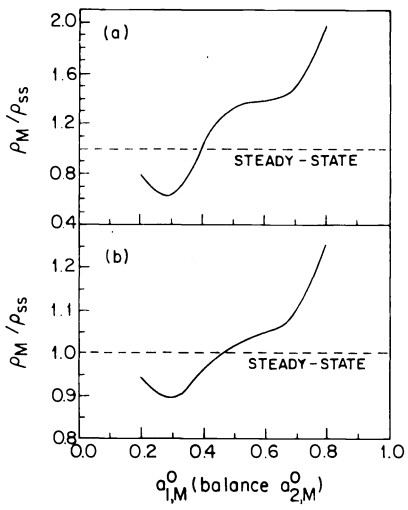

FIG. 12

Time-average production rates, ϱ_M, normalized with respect to the steady-state rates, ϱ_{SS}, as a function of the mean feed composition $a^0_{1,M}/a^0_{2,M}$; a Langmuir–Hinshelwood mechanism, $\tau_p = 50$, $\alpha = 0{\cdot}4$, $\gamma = 0{\cdot}5$, $\sigma^0 = 0{\cdot}03\ s^{-1}$; b Eley–Rideal mechanism $\tau_p = 20$, $\alpha = 0{\cdot}4$, $\gamma = 0{\cdot}5$, $\sigma^0 = 0{\cdot}03\ s^{-1}$

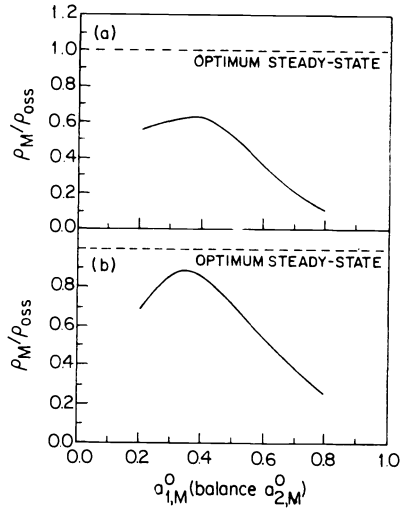

FIG. 13

Time-average production rates, ϱ_M, normalized with respect to the optimum steady-state rates, ϱ_{OSS}, as a function of the mean feed composition $a^0_{1,M}/a^0_{2,M}$; a Langmuir–Hinshelwood mechanism, $\tau_p = 50$, $\alpha = 0{\cdot}4$, $\gamma = 0{\cdot}5$, $\sigma^0 = 0{\cdot}03\ s^{-1}$; b Eley–Rideal mechanism $\tau_p = 20$, $\alpha = 0{\cdot}4$, $\gamma = 0{\cdot}5$, $\sigma^0 = 0{\cdot}03\ s^{-1}$

CONCLUSIONS

Binary reaction models have been used to show that forced feed composition cycling can result in a significant increase in the catalytic rate of product formation. However, at a constant space velocity of the reaction mixture, this enhanced rate appears never to exceed the maximum rate corresponding to the optimum steady-state feed composition. Cycling around a time-average feed composition equal to that of the optimum steady state leads to lower reaction rates. Reasons for this behaviour are to be found in the dynamics of the processes taking place on the catalyst surface and in the gas phase.

This study was extended to several other reaction stoichiometries, namely: $A + B \rightarrow C$, $2A + B_2 \rightarrow 2C$ and $A + 3B \rightarrow 2C$. The L–H and E–R mechanisms were considered and a wide range of rate constants combinations used. In all cases, the observations discussed above were found to apply. Another numerical study[11] of a periodically operated CSTR showed rate improvements for the CO oxidation but the calculations were carried out using feed compositions corresponding to suboptimal reaction rates. The CO oxidation system[11] shows that mutiple steady states are obtained. However, the highest time-average rates observed under cycling are still less than half the optimum steady-state rate.

In contrast to these numerical results, Jain et al[12], using a periodically operated CSTR observed experimentally that time-average ammonia production rates exceeded the optimum steady-state rate by 30%. In another esperimental study on CO methanation[13] forced feed composition cycling resulted in a significant improvement of reaction rate for any (including optimum) feed composition. Consequently, the simple L–H and E–R models appear to be unable to reproduce this behaviour. Of course, these models were derived for ideal surfaces, constant activity of catalyst and steady-state operation, for which the equations are very flexible and useful for empirical purposes. However, they fail when applied to a number of transient or cycling operations.

For this reason, there is a need to develop more sophisticated models for heterogeneous catalytic systems under dynamic operation. The models should be capable of predicting system states under forced cycling that are unattainable under steady-state operation. In one such attemptl Li et al,[14] introduced storage of a reaction intermediate at sites other than active ones plus a transport resistance between the interior of the catalyst and its outer surface in order to represent the ammonia data of Jain et al.[12]. An alternative approach was used in the experimental study of CO methanation[13] where the formation of a reactive carbonaceous deposits under unsteady-state conditions was assumed. Another possibility may be to introduce variable catalyst activity under dynamic operation into catalytic models.

The authors are grateful for support for this study through the Natural Sciences and Engineering Research Council of Canada in the form of an International Scientific Exchange Award (to K. K.) and operating grant (to R. R. H.).

SYMBOLS

a_i, a_j mole fraction of gaseous A_i, dimensionless surface concentration of A_j
A_i, A_j reaction component in the gas phase or on the catalyst surface respectively
c_i, c_j molar concentration of A_i, A_j
c_L total molar concentration of active sites, $1 . 10^{-4}$ mol g^{-1}
c_T total molar concentration in gas phase, $2{\cdot}437 . 10^{-5}$ mol cm^{-3}
k_i, k'_i rate constants
t time
V reactor free volume, 10 cm^3
W catalyst weight, 5 g
α amplitude
γ cycle split
ϕ capacity factor (see Table I)
$\varkappa_i$, $\varkappa'_i$ dimensionless rate constants (see Table III)
ϱ normalized rate of product formation (Eqs (*7*) and (*8*))
ϱ_i, ϱ_j dimensionless rate of formation of A_i, A_j (see Table II)
σ space velocity of reaction mixture
τ dimensionless time (see Table I)
τ_p cycle period

Subscripts

1, 2, 3 identifiers for gas components A, B, C
4, 5, 6 identifiers for surface components S, A . S, B_2 . S
I, II first and second part of the period
M time-average value in the cycle
OSS optimum steady state
SS steady state

Superscript

0 reactor input

REFERENCES

1. Bailey J. E. in: *Chemical Reactor Theory: A Review* (L. Lapidus and N. R. Amundson, Eds), Chap. 12. Prentice Hall, Englewood Cliffs 1977.
2. Silveston P. L., Hudins R. R. in: *Recent Trends in Chemical Reaction Engineering*, Vol. I, p. 235. (*Proc. Second Int. Chem. React. Eng. Conf., Pune, 1987*).
3. Schädlich K., Hoffmann U., Hofmann H.: Chem. Eng. Sci. *38*, 1375 (1983).
4. Nowobilski P. J., Takoudis C. G.: Chem. Eng. Commun. *40*, 249 (1986).
5. Klusáček K., Silveston P. L., Hudgins R. R.: Can. J. Chem. Eng. *67*, 615 (1989).
6. *Library of Standard Fortran Routines*, IMSL, Release 1980. IMSL Inc., Houston, Texas, USA.
7. Hindmarsh A. C.: *GEAR: Ordinary Differential Equation System Solver*. Lawrence Livermore Laboratory, Report UCID-30 001, Revision 3, (1974).
8. Horn F. J. M., Bailey J. E.: J. Optim. Theor. Appl. *2*, 441 (1968).
9. Matsubara M., Nishimura Y., Takahashi N.: Chem. Eng. Sci. *28*, 1369 (1973).

10. Wilson H. D., Rinker R. G.: Chem. Eng. Sci. *37*, 343 (1982).
11. Lynch D. T.: Can J. Chem. Eng. *61*, 183 (1983).
12. Jain A. K., Hudgins R. R., Silveston P. L.: Can. J. Chem. Eng. *63*, 803 (1983).
13. Stuchlý V., Klusáček K. in: *Unsteady State Processes in Catalysis*, p. 423. *(Proceedings of the International Conference, Novosibirsk, 1990;* Yu. Sh. Matros, Ed.).
14. Li C., Hudgins R. R., Silveston P. L.: Can. J. Chem. Eng. *61*, 824 (1983).

Translated by the author (K. K.).